Extension of the Bjorken Formula for Relativistic Heavy Ion Collisions

Zi-Wei Lin
Department of Physics, East Carolina University, Greenville, NC 27858, USA and
Key Laboratory of Quarks and Lepton Physics (MOE) and Institute of Particle Physics,
Central China Normal University, Wuhan 430079, China

For relativistic heavy ion collisions, the Bjorken formula is very useful for the estimation of the initial energy density once an initial time τ_0 is specified. However, the formula is only valid when τ_0 is much bigger than the finite time it takes for the two nuclei to cross each other, therefore it cannot be trusted at low energies, below $\sqrt{s_{\rm NN}} \sim 50$ GeV for central Au+Au collisions. In this study we extend the Bjorken formula by including a time profile for the initial energy production. Analytical solutions for the formed energy density as functions of time are derived for several time profiles, and we find that at low energies they are much less sensitive to the uncertainty of the formation time. Compared to the Bjorken formula, the maximum energy density are much lower while the width of the energy density time evolution is much bigger at low energies. Comparisons with results from a multi-phase transport confirm the key features of these solutions. This work thus provides a general model for the initial energy production of relativistic heavy ion collisions, especially at low energies.

arXiv:1704.08418v1 [nucl-th] 27 Apr 2017

I. Introduction. Relativistic heavy ion collisions aim to create the quark-gluon plasma (QGP) and study its properties [1, 2]. Therefore it is important to better understand the initial energy production, including the maximum value and time evolution of the energy density in the overlap volume. For low energies such as the Beam Energy Scan at the Relativistic Heavy Ion Collider, the relationship between the time evolution of the energy density or net-baryon density and the possible critical point of QCD becomes important [3, 4]. The Bjorken formula [5] is a very useful tool in estimating the initial energy density at mid-rapidity right after the two nuclei pass each other:

$$\epsilon_{\rm Bj}(t) = \frac{1}{A_{\rm T}\, t}\frac{dE_{\rm T}}{dy}. \tag{1}$$

In the above, $A_{\rm T}$ represents the full transverse area of the overlap volume, and $dE_{\rm T}/dy$ is the rapidity density of the transverse energy at mid-rapidity (at an early time t), which is often approximated with the experimental $dE_{\rm T}/dy$ value in the final state. Since the Bjorken energy density diverges as $t \to 0$, a finite value is needed for the initial time τ_0 [2]. Considering that the production of a particle takes a finite formation time $\tau_{\rm F}$, one can take the Bjorken formula at time $\tau_{\rm F}$ to obtain the initial formed energy density.

A severe limitation of the Bjorken formula results from the fact that it neglects the finite thickness of the colliding nuclei (along the beam direction z), which leads to a finite duration time for the initial energy production. Using a hard-sphere model for the nucleus, it will take the following time for two nuclei of the same atomic weight A to cross each other in a central collision in the center-of-mass frame [6]:

$$d_t = \frac{2R_A}{\sinh y_{\rm CM}}, \tag{2}$$

where $y_{\rm CM}$ is the projectile rapidity in the center-of-mass frame and R_A is the nuclear radius. Therefore the Bjorken formula is only valid when the duration time (or crossing time) is much smaller than the formation time $\tau_{\rm F}$ [2]. As an example, for $\tau_0 = 0.5$ fm/c, the Bjorken formula cannot be applied for central Au+Au collisions below $\sqrt{s_{\rm NN}} = 50$ GeV since $d_t \approx 0.5$ fm/c there.

Our goal of this study is to derive a Bjorken-like formula so that it is also valid at low energies where the Bjorken formula breaks down. We accomplish this by including the finite crossing time in the time profile of the initial energy production. We focus on the formed energy density, averaged over the full transverse overlap area, at mid-rapidity in the center-of-mass frame of central collisions of two identical nuclei.

II. Method. The Bjorken formula assumes that the initial energy production at rapidity $y = 0$ only occurs at time $t = 0$ on the $z = 0$ plane. Considering the finite crossing time of the two nuclei, the initial energy production actually goes on throughout this period of time; therefore let us write the production rate of the initial transverse energy rapidity density at time x as $d^2E_{\rm T}/dy/dx$. Figure 1 shows a schematic picture, where the two nuclei come into contact at time 0 and pass each other at time d_t. Thus there could be particle productions at any time $x \in [0, d_t]$, while $d^2E_{\rm T}/dy/dx = 0$ for $x < 0$ or $x > d_t$. The two diagonal lines in Fig. 1 represent the light-cone boundaries; and we neglect the possible finite width in z for the initial energy production, except for the results from a multi-phase transport (AMPT) model [7]. To obtain analytical results, we make minimal extensions to the Bjorken formula framework [5], thus we also assume massless particles and neglect secondary particle interactions or the transverse expansion.

Let us evaluate the energy density within a narrow region $-d \le z \le d$ at time $t > d_t$. For a particle produced at time x to stay within this z-region, its rapidity (or pseudo-rapidity) needs to satisfy

$$|\tanh y| \approx |y| \le \frac{d}{t-x} \tag{3}$$

at $y \sim 0$. Note that the right-hand-side above can al-

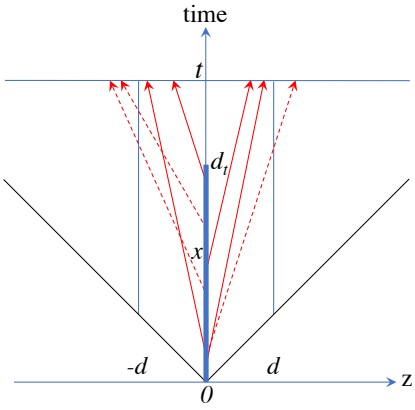

FIG. 1: Particles around zero rapidity could be produced at any time x within $[0, d_t]$ and propagate to observation time t.

ways be made small with small-enough d. Therefore the average energy density in this region at time t is

$$\frac{E}{2dA_{\rm T}} = \frac{1}{A_{\rm T}}\int_0^{d_t} \frac{d^2E_{\rm T}}{dy\,dx}\frac{dx}{(t-x)}. \tag{4}$$

From now on we shall study the formed energy density by assuming a finite formation time $\tau_{\rm F}$ for the produced particles. A similar analysis gives the following average formed energy density at any time $t \geq \tau_{\rm F}$ as

$$\epsilon(t) = \frac{1}{A_{\rm T}}\int_0^{t-\tau_{\rm F}} \frac{d^2E_{\rm T}}{dy\,dx}\frac{dx}{(t-x)}. \tag{5}$$

As in the Bjorken formula, $\epsilon(t < \tau_{\rm F}) = 0$. However, an important feature of the above formula is that it applies to early times when the two nuclei are still crossing each other (i.e. $t \leq d_t + \tau_{\rm F}$). To proceed further, we will next take specific forms for the time profile of the initial energy production $d^2E_{\rm T}/dy/dx$.

III. Results. For simplicity, we first assume that the initial energy is produced uniformly from time t_1 to t_2 (with $t_{21} \equiv t_2 - t_1$):

$$\frac{d^2E_{\rm T}}{dy\,dx} = \frac{1}{t_{21}}\frac{dE_{\rm T}}{dy},\ \text{if } x \in [t_1, t_2]. \tag{6}$$

Note that we only need the above assumption to apply at $y \sim 0$. Also, we have not related t_1 and t_2 to d_t for the sake of generality. An illustration of this time profile is shown as the dashed curve in Fig. 2. Equation (5) then gives the following solution for the formed energy density:

$$\begin{aligned}\epsilon_{\rm uni}(t) &= \frac{1}{A_{\rm T}t_{21}}\frac{dE_{\rm T}}{dy}\ln\left(\frac{t-t_1}{\tau_{\rm F}}\right), \text{if } t \in [t_1+\tau_{\rm F}, t_2+\tau_{\rm F}];\\ &= \frac{1}{A_{\rm T}t_{21}}\frac{dE_{\rm T}}{dy}\ln\left(\frac{t-t_1}{t-t_2}\right), \text{if } t \geq t_2+\tau_{\rm F}.\end{aligned} \tag{7}$$

One can easily verify that, for $t_1 = 0$ and $t_2/\tau_{\rm F} \to 0$, this solution reduces to the Bjorken formula of Eq.(1).

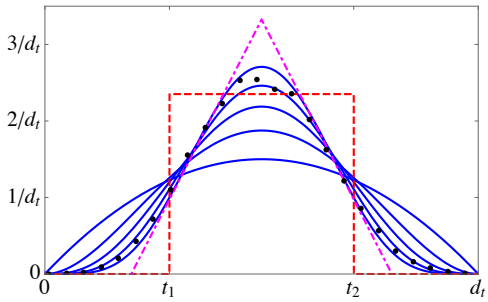

FIG. 2: Time profiles for the initial energy production at mid-rapidity: a uniform profile (dashed curve), beta profiles with integer powers $n = 1$ to 5 (solid curves), and a triangular profile (dot-dashed). Circles represent the time profile of partons within mid-spacetime-rapidity from the string melting AMPT model for central Au+Au collisions at $\sqrt{s_{\rm NN}} = 11.5$ GeV.

Qualitatively, this energy density starts from 0 at time $t_1 + \tau_{\rm F}$, grows smoothly to the following maximum value ϵ^{max} at time $t_2 + \tau_{\rm F}$, and then decreases abruptly after the energy production stops:

$$\epsilon^{max}_{\rm uni} = \epsilon_{\rm uni}(t_2+\tau_{\rm F}) = \frac{1}{A_{\rm T}t_{21}}\frac{dE_{\rm T}}{dy}\ln\left(1+\frac{t_{21}}{\tau_{\rm F}}\right). \tag{8}$$

Compared to the maximum energy density $\epsilon_{\rm Bj}(\tau_{\rm F})$ given by the Bjorken formula, we have

$$\frac{\epsilon^{max}_{\rm uni}}{\epsilon_{\rm Bj}(\tau_{\rm F})} = \frac{\tau_{\rm F}}{t_{21}}\ln\left(1+\frac{t_{21}}{\tau_{\rm F}}\right). \tag{9}$$

Therefore the ϵ^{max} value above is always smaller than the Bjorken initial energy density: $\epsilon^{max} \ll \epsilon_{\rm Bj}(\tau_{\rm F})$ at low energies where $\tau_{\rm F}/t_{21}$ is small, while at high energies $\epsilon^{max} \approx \epsilon_{\rm Bj}(\tau_{\rm F})$. Furthermore, as $\tau_{\rm F}/t_{21} \to 0$, the peak energy density ϵ^{max} grows as $\ln(1/\tau_{\rm F})$, much slower than the $1/\tau_{\rm F}$ growth of the Bjorken formula. This means that, after taking into account the finite crossing time, the maximum energy density achieved will be much less sensitive to the uncertainty of $\tau_{\rm F}$, especially at lower energies where $t_{21} \sim \mathcal{O}(d_t)$ is bigger. In addition, Eq.(7) shows that the initial energy density at time later than $t_2 + \tau_{\rm F}$ is independent of $\tau_{\rm F}$. We shall see that these features are general and also apply to the other time profiles.

Due to the typical spherical shape of a nucleus, there will be few primary nucleon-nucleon interactions when the two nuclei barely touch or almost pass each other, while there will be many such interactions when the two nuclei fully overlap (around time $d_t/2$). We thus expect the time profile of the initial energy production to peak around time $d_t/2$ while diminish at time 0 and d_t. Therefore we can choose the following time profile based on the probability density function of the beta distribution with equal shape parameters:

$$\frac{d^2E_{\rm T}}{dy\,dx} = a_n\left[x(d_t-x)\right]^n\frac{dE_{\rm T}}{dy},\ \text{if } x \in [0, d_t]. \tag{10}$$

In the above, power n does not need to be an integer, and $a_n = 1/d_t^{2n+1}/B(n+1,n+1)$ is the normalization factor with $B(\alpha,\beta)$ being the Beta function. This smooth beta profile reduces to a uniform profile when $n=0$; with an appropriate value of n it can also well describe the transport model time profile, as shown in Fig. 2. We obtain the following solution for the formed energy density:

$$\begin{aligned}\epsilon_{\rm beta}(t) &= \frac{1}{A_{\rm T}}\frac{dE_{\rm T}}{dy}\frac{[(t-\tau_{\rm F})/d_t]^{n+1}}{(n+1)B(n+1,n+1)\,t} \\ &\quad *F_1\left[n+1,-n,1,n+2,\frac{t-\tau_{\rm F}}{d_t},\frac{t-\tau_{\rm F}}{t}\right], \\ &\quad \text{if } t\in[\tau_{\rm F},d_t+\tau_{\rm F}]; \\ &= \frac{1}{A_{\rm T}}\frac{dE_{\rm T}}{dy}\frac{1}{t} *{}_2F_1\left[1,n+1,2n+2,\frac{d_t}{t}\right], \\ &\quad \text{if } t\geq d_t+\tau_{\rm F}. \end{aligned} \tag{11}$$

F_1 above is the Appell hypergeometric function of two variables, and ${}_2F_1$ is the Gaussian hypergeometric function. One can verify that for $n=0$ the above solution reduces to Eq.(7) for $t_1=0$ & $t_2=d_t$.

We now apply these solutions to central Au+Au collisions. The nuclear transverse area is taken as

$$A_{\rm T} = \pi R_A^2, \text{ with } R_A = 1.12A^{1/3} \text{ fm}, \tag{12}$$

where $A=197$. We take the mid-rapidity $dE_{\rm T}/dy$ as the following data-based parameterization [8]:

$$\frac{dE_{\rm T}}{dy} = 1.25\frac{dE_{\rm T}}{d\eta} = 0.913N_{\rm part}\ln\left(\frac{\sqrt{s_{\rm NN}}}{2.35}\right), \tag{13}$$

where $\sqrt{s_{\rm NN}}$ must be greater than 2.35 in the unit of GeV. Also, we take $N_{\rm part}=A$ for central collisions.

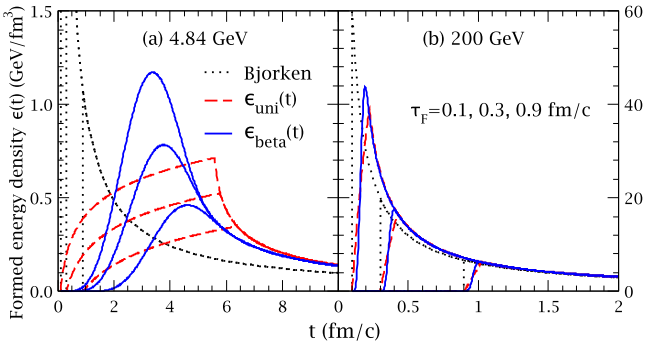

FIG. 3: Average formed energy densities at mid-rapidity as functions of time for central Au+Au collisions at (a) 4.84 GeV and (b) 200 GeV from the uniform time profile with the naive choice of $t_1=0$ & $t_2=d_t$ (dashed), the beta time profile for $n=4$ (solid), and the Bjorken formula (dotted). Three sets of curves of each type correspond to $\tau_{\rm F}=0.1, 0.3$ & 0.9 fm/c.

Our results for central Au+Au collisions at $\sqrt{s_{\rm NN}}=$ 4.84 GeV and 200 GeV are shown in Fig. 3 for different formation times $\tau_{\rm F}=0.1, 0.3$ & 0.9 fm/c. Also shown are the results implied by the Bjorken formula: $\epsilon_{\rm Bj}(t) = 1/(A_{\rm T}t)dE_{\rm T}/dy$ for $t\geq\tau_{\rm F}$ (and $=0$ for $t<\tau_{\rm F}$). We have taken $n=4$ for the beta profile according to Fig. 2, and we take the naive choice of $t_1=0$ and $t_2=d_t$ for the uniform profile in Fig. 3. At 4.84 GeV, we see that the time evolution of the energy density in either time profile has a much bigger width (e.g. full width at half maximum) than the Bjorken results, while the maximum energy density is much lower than the corresponding Bjorken value for the same $\tau_{\rm F}$. As expected, our maximum initial energy density ϵ^{max} changes by a much smaller factor of 2.1 (uniform profile) or 2.5 (beta profile) when $\tau_{\rm F}$ changes from 0.1 to 0.9 fm/c; while the Bjorken initial energy density changes by a factor of 9. On the other hand, our results at 200 GeV are much closer to (although still different from) the Bjorken results; this is expected since the crossing time there ($d_t\approx 0.12$ fm/c) is very small. For both energies, our results approach the Bjorken results at late times.

Both the Bjorken formula and our method have neglected secondary particle interactions and the transverse expansion, which could affect the time evolution of the energy density. These dynamics can be described by transport models such as AMPT [7] or hydrodynamical models [9, 10]. Now we compare our analytical solutions with results from the string melting AMPT model, which includes a conversion of excited strings into a parton matter, partonic scatterings, a quark coalescence for hadronization, and hadronic scatterings. For this study, the string melting AMPT model [7] has been improved by including the finite thickness of nuclei [11], then we calculate the average local energy density (over the hard-sphere transverse area $A_{\rm T}$) for partons at mid-spacetime-rapidity following the method of an earlier study [12]. Circles in Fig. 2 represent the distribution of production time of partons within mid-spacetime-rapidity from AMPT for central ($b=0$ fm) Au+Au collisions at $\sqrt{s_{\rm NN}}=11.5$ GeV [11]. We thus take $n=4$ for the beta time profile, since this can reasonably describe the AMPT time profile. To get the same mean and standard deviation as the beta profile, we set $t_1=0.29d_t$ & $t_2=0.71d_t$ for the uniform profile.

Figure 4 shows our results from different time profiles together with the Bjorken results at different energies. We see from Figs. 4(a)&(d) that, unlike Figs. 3, results from the uniform and beta profiles here are quite close to each other once the uniform profile is set to the same mean and standard deviation as the beta profile. Curves with filled and open circles are respectively the AMPT results with and without the finite nuclear thickness (after small shifts in time that help account for the difference between the Woods-Saxon distribution and the hard-sphere model of the nucleus). Note that the AMPT results are generally wider in time; partly because the parton formation time in AMPT is not set as a constant but is inversely proportional to the parent hadron transverse mass [7]; we find that the parton formation time distribution at mid-spacetime-rapidity has a mean value of ~ 0.3 fm/c but has a long tail. Secondary parton scat-

terings and the transverse expansion in AMPT can also cause differences from the analytical results. Overall, we see that the AMPT results without considering the finite nuclear thickness are similar to the Bjorken results, while the AMPT results including the finite thickness are similar to our analytical results.

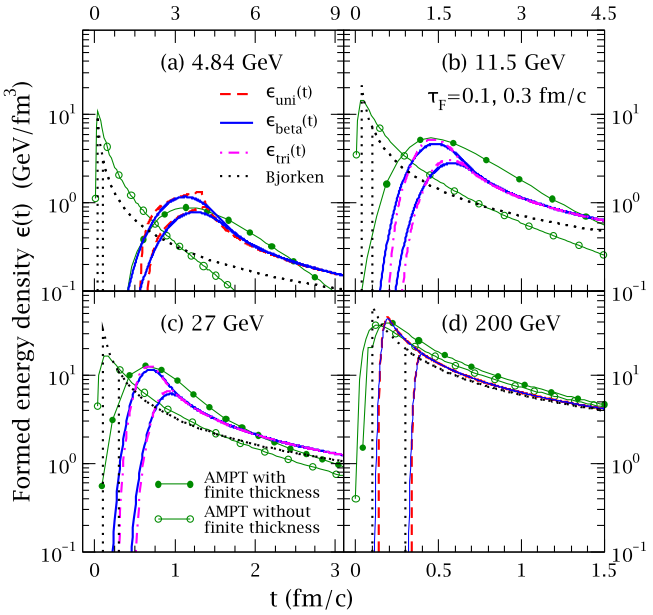

FIG. 4: Results for the uniform (dashed curves), beta (solid curves), triangular (dot-dashed curves) time profiles and the Bjorken formula (dotted curves) for $\tau_{_F} = 0.1$ & 0.3 fm/c, in comparison with the corresponding AMPT results (circles), for central Au+Au collisions at (a) 4.84 GeV, (b) 11.5 GeV, (c) 27 GeV, and (d) 200 GeV.

IV. Discussions. We can also take a triangular time profile, as illustrated by the dot-dashed curve in Fig. 2, from time t_1 to t_2 with the peak at $t_{mid} \equiv (t_1 + t_2)/2$: $d^2E_{_T}/dy/dx \propto (x - t_1)$ for $t \in [t_1, t_{mid}]$ while $\propto (t_2 - x)$ for $t \in [t_{mid}, t_2]$. We then obtain the following solution:

$$\begin{aligned}\epsilon_{\rm tri}(t) &= \frac{4}{A_{_T} t_{21}^2}\frac{dE_{_T}}{dy}\left[-t + t_1 + \tau_{_F} + (t - t_1)\ln\left(\frac{t - t_1}{\tau_{_F}}\right)\right], \\ &\quad \text{if } t \in [t_1 + \tau_{_F}, t_{mid} + \tau_{_F}]; \\ &= \frac{4}{A_{_T} t_{21}^2}\frac{dE_{_T}}{dy}\left[t - t_2 - \tau_{_F} + (t - t_1)\ln\left(\frac{t - t_1}{t - t_{mid}}\right)\right. \\ &\quad \left. + (t_2 - t)\ln\left(\frac{t - t_{mid}}{\tau_{_F}}\right)\right], \text{if } t \in [t_{mid} + \tau_{_F}, t_2 + \tau_{_F}]; \\ &= \frac{4}{A_{_T} t_{21}^2}\frac{dE_{_T}}{dy}\left[(t - t_1)\ln\left(\frac{t - t_1}{t - t_{mid}}\right)\right. \\ &\quad \left. + (t_2 - t)\ln\left(\frac{t - t_{mid}}{t - t_2}\right)\right], \text{ if } t \geq t_2 + \tau_{_F}. \end{aligned} \tag{14}$$

This energy density increases smoothly to the following maximum value ϵ^{max} at a time within $(t_{mid} + \tau_{_F}, t_2 + \tau_{_F})$ and then decreases smoothly with time:

$$\begin{aligned}\epsilon_{\rm tri}^{max} &= \epsilon_{\rm tri}\Big((t_1 + t_2 + \tau_{_F} + \sqrt{\tau_{_F}}\sqrt{2\,t_{21} + \tau_{_F}}\,)/2\Big) \\ &= \frac{2}{A_{_T} t_{21}}\frac{dE_{_T}}{dy}\left[\,-1 - \frac{\tau_{_F}}{t_{21}} + \sqrt{\frac{\tau_{_F}}{t_{21}}}\sqrt{2 + \frac{\tau_{_F}}{t_{21}}}\right. \\ &\quad \left. + 2\ln\left(\frac{1 + \sqrt{1 + 2\,t_{21}/\tau_{_F}}}{2}\right)\right]. \end{aligned} \tag{15}$$

Figures 4(b)&(c) show that results from the beta and triangular profiles are almost identical in shape and close in magnitudes, after we set $t_1 = 0.20 d_t$ & $t_2 = 0.80 d_t$ for the triangular time profile to have the same mean and standard deviation as the beta profile for $n = 4$. An advantage of the triangular profile is that we have analytical expressions for its ϵ^{max} and the corresponding time.

We have only addressed the energy density averaged over the full transverse overlap area $A_{_T}$. Note that the transverse overlap area at time before $d_t/2$ is smaller due to the partial overlap of the two nuclei. To average over this partial overlap area, one may replace $A_{_T}$ in our solutions by $A_{_T}[1 - (1 - 2t/d_t)^2]$ for $t \leq d_t/2$. This will enhance the energy density somewhat at early times.

Our analytical method includes the finite time duration but neglects the possible finite width in z for the initial energy production. Results from the AMPT model [11] indicate a finite width in z, which effect is already included in the AMPT results here; further work may be warranted to include this effect analytically. We also note that the finite duration of proper time in the initial energy production has been considered in hydrodynamical models [13, 14], where an energy source term with a finite time duration can be introduced and our method can be applied to help describe the initial stage.

V. Conclusions. We have extended the Bjorken formula by including a time profile for the initial energy production due to the finite nuclear thickness. We have considered a simple uniform as well as more realistic time profiles, and analytical solutions of the formed energy density have been obtained that are also valid at low energies where the Bjorken formula breaks down. At late times, the solution of the energy density approaches the Bjorken formula. We then apply the solutions to central Au+Au collisions in the energy range $\sqrt{s_{_{NN}}} \in [4.84, 200]$ GeV. After taking into account the finite crossing time, the maximum energy density achieved is much less sensitive to the uncertainty of $\tau_{_F}$, especially at lower energies where the crossing time is bigger. At low energies, the energy density reaches a much lower maximum value than the Bjorken energy density for the same formation time $\tau_{_F}$, but the width of the time evolution of energy density is much bigger. In addition, comparisons with the results from the string melting AMPT model confirm the key features of the analytical solutions. Therefore this extension provides a convenient tool to model the initial energy production in relativistic heavy ion collisions, especially at low energies $\sqrt{s_{_{NN}}} <\sim 50$ GeV.

We thank Miklos Gyulassy for careful reading of the manuscript and helpful comments. This work is supported in part by National Natural Science Foundation of China grant No. 11628508.

[1] J. Adams *et al.* [STAR Collaboration], Nucl. Phys. A **757**, 102 (2005).
[2] K. Adcox *et al.* [PHENIX Collaboration], Nucl. Phys. A **757**, 184 (2005).
[3] M. A. Stephanov, Phys. Rev. Lett. **107**, 052301 (2011).
[4] A. Bialas, A. Bzdak and V. Koch, arXiv:1608.07041 [hep-ph].
[5] J. D. Bjorken, Phys. Rev. D **27**, 140 (1983).
[6] K. Kajantie, R. Raitio and P. V. Ruuskanen, Nucl. Phys. B **222**, 152 (1983).
[7] Z. W. Lin, C. M. Ko, B. A. Li, B. Zhang and S. Pal, Phys. Rev. C **72**, 064901 (2005).
[8] S. S. Adler *et al.* [PHENIX Collaboration], Phys. Rev. C **71**, 034908 (2005); *ibid* **71**, 049901 (2005) (E).
[9] C. Shen and U. Heinz, Phys. Rev. C **85**, 054902 (2012), *ibid* **86**, 049903 (2012) (E).
[10] D. Oliinychenko, P. Huovinen and H. Petersen, Phys. Rev. C **91**, no. 2, 024906 (2015).
[11] Z.W. Lin, in preparation.
[12] Z. W. Lin, Phys. Rev. C **90**, no. 1, 014904 (2014).
[13] M. Okai, K. Kawaguchi, Y. Tachibana and T. Hirano, arXiv:1702.07541 [nucl-th].
[14] C. Shen, G. Denicol, C. Gale, S. Jeon, A. Monnai and B. Schenke, arXiv:1704.04109 [nucl-th].